
SYNTHESIS AND PROPERTIES OF INORGANIC COMPOUNDS

Synthesis and Doping of Zinc Sulfide in a Homogeneous System Based on Dodecane, Its Identification and Optical Properties

M. A. Zarudskikh^a, E. G. Ilina^a, A. S. Mankevich^b, and V. P. Smagin^{a, *}

^aAltai State University, Barnaul, 656049 Russia

^bZAO SuperOx, Moscow, 117246 Russia

*e-mail: smaginV@yandex.ru

Received September 6, 2023; revised October 18, 2023; accepted October 28, 2023

Abstract—Zinc sulfide doped with Mn²⁺ ions was synthesized in a homogeneous dodecane medium using the emerging reagent method. Using the methods of chemical analysis, X-ray powder diffraction, IR spectroscopy, and electron microprobe microscopy, the products were identified and photographs of the surface of powder particles (SEM) were obtained. Based on the results obtained, it was concluded that nano-sized objects are formed that have a polytype structure with a predominance of distorted cubic crystals, forming agglomerates up to 10 μm in size in ZnS powder and up to 100 μm in ZnS–Mn powder. The formation of nanosized ZnS particles is confirmed by spectral data. The influence of manganese ions on the photoluminescence (PL) of the powder manifests itself in a change in the type of the descending branch of the ZnS–Mn PL band; this is associated with recombination processes at the levels of defects formed by Mn²⁺ ions in the ZnS structure at their low concentration.

Keywords: zinc sulfide, doping, manganese(II) ions, non-aqueous homogeneous synthesis, dodecane, photoluminescence

DOI: 10.1134/S0036023623602969

INTRODUCTION

Metal sulfides are widely used as the basis for luminescent materials of different luminescence colors in radio electronics, electro-optics, computing and measuring technology [1–3]. Particular attention of researchers is directed to the development of complex semiconductor structures in the nanoscale range [1, 3, 4]. A popular phosphor, as well as one of the promising semiconductor components of matrices of semiconductor structures, is zinc sulfide. Individual and doped coarse-crystalline and nano-sized ZnS powders, films, and complex structures [5–13] are of scientific and practical interest. Bulk ZnS has been well studied and is used in optical instrumentation as electroluminophores and photoluminophores [1, 3, 8, 14, 15]. Its luminescence is determined by the defectiveness of the crystals. The atomic ratio S^{2−}/Zn²⁺ is of great importance. The authors [16] note that the maximum luminescence intensity of ZnS is achieved with a double excess of sulfur ions over zinc ions. The luminescence spectrum of ZnS depends on doping with metal ions, the state of the particle surface, as well as external factors [7, 14, 17, 18]. The action of the entire complex of factors determines the structure and morphology of ZnS crystals. To construct the energy diagram of ZnS, the Schon–Klasens and Lambe–Klick schemes are used [19, 20].

Mn²⁺ ions are introduced into the ZnS matrix as optical and magnetic modifiers [1, 3, 21, 22]. In the photoluminescence (PL) spectra of ZnS–Mn²⁺, a ${}^4T_1 \rightarrow {}^6A_1$ band of the electronic transition of Mn²⁺ ions is observed [15, 22, 23]. It overlaps with the long-wavelength recombination PL bands of ZnS. At low concentrations of Mn²⁺ ions, the mechanism of resonant energy transfer of the semiconductor matrix to the excited energy levels of manganese ions operates. With increasing Mn²⁺ concentration, the “electronic” mechanism dominates. It is associated with electron transitions between the “own” energy levels of Mn²⁺ ions. Upon direct excitation of Mn²⁺ ions, with the maxima of their absorption bands located in the wavelength range 390–535 nm, a “manganese” luminescence band is observed in the PL spectra of ZnS–Mn²⁺ [24]. In addition, Mn²⁺ ions are introduced into the structure of the semiconductor matrix creating defects, the levels of which participate in recombination processes.

The optical properties of semiconductor structures depend on the composition and structures of activator centers, which are formed during the synthesis process and depend on its conditions [1, 3, 14, 15]. Various methods for obtaining metal sulfides are described in the literature [1, 5, 8, 12, 13, 24–27]. Hydrogen sulfide, sodium sulfide, and organic sulfur-containing

compounds are used as sulfidizers. One of the disadvantages of synthesis based on precipitation with hydrogen sulfide or sodium sulfide from aqueous solutions of metal salts is the formation of amorphous or partially crystalline precipitates containing hydroxo forms of the products. As a result of hydrothermal synthesis, hydrolysis of the target products may occur; in some cases, they cannot be isolated at all. In addition, this synthesis method involves the use of high temperatures and pressures, which requires the process to be carried out in an autoclave. Sol-gel technologies are also used to synthesize semiconductor structures, and various versions of the Langmuir–Blodgett method are used to obtain films [1, 28]. At the initial stage of synthesis, in some cases, colloidal solutions are formed [29–31]. When synthesizing powders, their formation complicates purification and sometimes leads to difficulties in obtaining a monophasic product. Supplying gaseous hydrogen sulfide into the reaction medium is low-tech and not environmentally friendly. When using sodium sulfide, the results of the synthesis largely depend on the acidity of the medium.

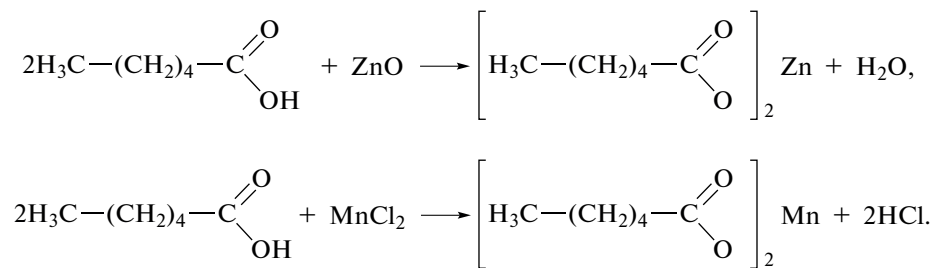
Methods for the synthesis of metal sulfides based on the reactions of metal salts with hydrogen sulfide in a saturated hydrocarbon environment are described [31–37]. Hydrogen sulfide is formed directly in the reaction medium of the saturated hydrocarbon during its reaction with dissolved elemental sulfur. When carrying out the synthesis, metal nitrates, acetates, and trifluoroacetates are used [31–34]. Schemes of synthesis and equations of chemical reactions occurring during its implementation were reported [34, 37]. It should be noted that in most cases, reaction systems are heterogeneous. This is explained by the negligible

solubility of the metal salts used in non-polar saturated hydrocarbons. This significantly complicates the synthesis and purification of products and prevents the uniform distribution of components, especially alloying ones, in the reaction system, and, consequently, in the synthesis products. Unlike the above salts, metal alkanoates dissolve quite well in saturated hydrocarbons with the number of carbon atoms in the hydrocarbon chain >5 . The authors [32–34, 37] presented the identification results and determined the yield of the products of these synthesis. However, the optical properties of sulfides, as well as the possibility of using this method of synthesis and doping to obtain structures for optoelectronic applications, have practically not been studied.

The purpose of this work is to carry out the non-aqueous synthesis of zinc sulfide doped with Mn^{2+} ions in a homogeneous medium by reacting metal hexanoates with hydrogen sulfide formed during the reaction of elemental sulfur with dodecane, which is also a reaction medium for the production of metal sulfides, and to study its properties.

EXPERIMENTAL

Salts of hexanoic (caproic) acid $CH_3(CH_2)_4COOH$ were used as metal sulfide precursors. Zinc and manganese hexanoates were synthesized according to the method [38] by reacting metal oxide and chloride with a twofold excess of hexanoic acid, which was both a reagent and a reaction medium, at its boiling point of $205^\circ C$ for 1.5 h:



Hexanoic acid was preliminarily purified by simple distillation at atmospheric pressure. Purity was monitored by boiling point, refractive index, and IR spectra. The resulting salt precipitates were filtered off, washed with hot hexane to remove acid residues, and dried in air. Hexane was preliminarily purified from the possible presence of peroxide compounds according to the procedure [39]. As a result, colorless crystalline compounds were obtained, which were identified by chemical and IR spectroscopic analysis. IR spectra of salts (Fig. 1) were recorded on an InfralumFT 801

IR Fourier spectrometer in the wavenumber range of 4000 – 500 cm^{-1} using KBr tablets.

The content of metals in metal hexanoates was determined by complexometric titration according to the methods reported [40, 41]. The zinc content was $(21.9 \pm 0.2)\%$ with a theoretical content of 22.1% in the compound of composition $Zn(C_5H_{11}COO)_2$; the manganese content in manganese hexanoate was $(17.6 \pm 0.2)\%$ with a theoretical content of 17.3% in the $Mn(C_5H_{11}COO)_2$ compound.

Zinc sulfide was synthesized according to the method reported [37] by reacting zinc hexanoate with

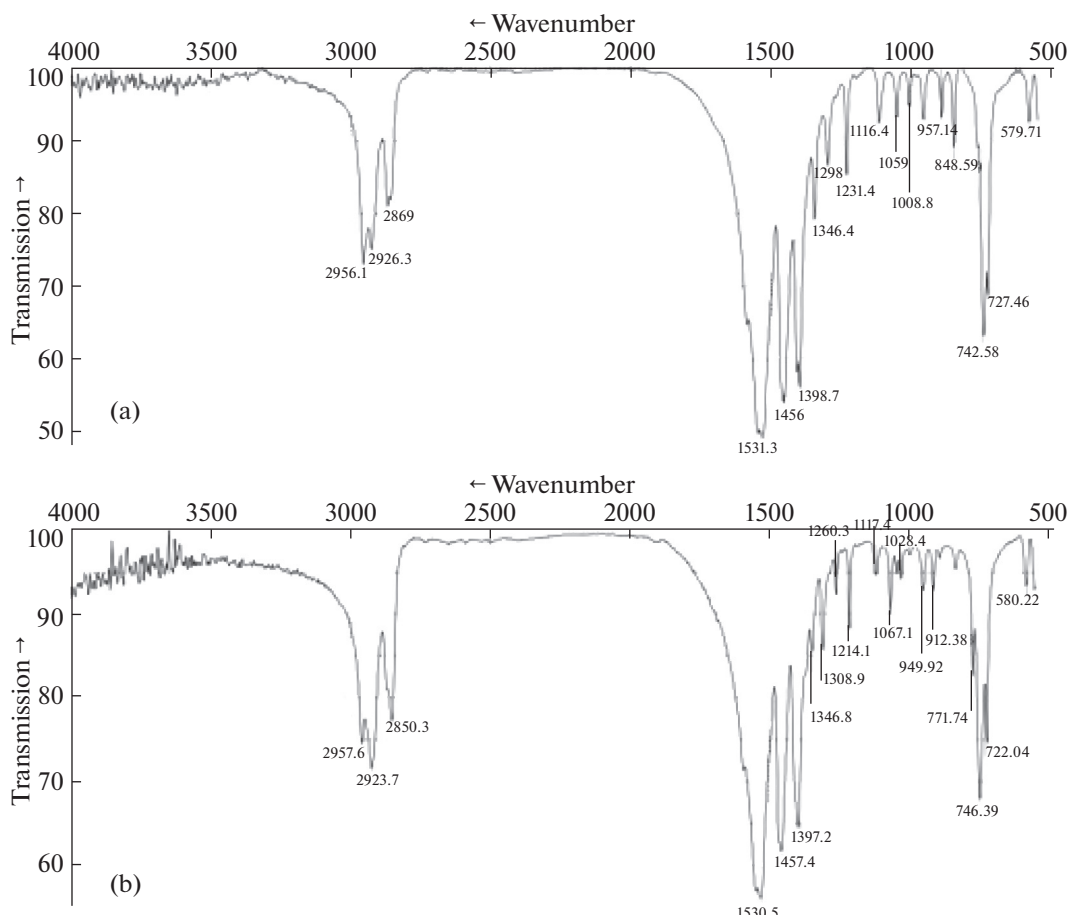
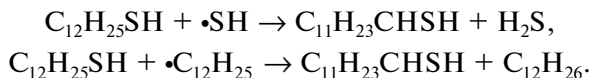
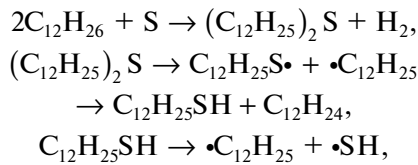


Fig. 1. IR spectra of (a) zinc and (b) manganese(II) hexanoates (KBr tablets).

hydrogen sulfide in dodecane at a dodecane boiling point of 216°C for 3.5 h. Dodecane (pure grade, Russian State Standard) was preliminarily purified by distillation according to the procedure [39]. Hydrogen sulfide was formed directly in the reaction medium during the reaction of elemental sulfur (special quality grade, Russian State Standard) with dodecane. Similar to work [34], where the radical chain mechanism of the reaction between sulfur and *n*-hydrocarbons with the formation of hydrogen sulfide is described using *n*-decane as an example, we present the sequence of the corresponding reactions:



The products of the interaction of sulfur with *n*-alkanes are thiols and organic sulfides. As a result of

the reaction of thiols and sulfides, as well as their thermal destruction, hydrogen sulfide is formed [34].

During the reaction, the color of the initial solution changed and a white crystalline precipitate characteristic of zinc sulfide was formed. At the initial stage of the reaction, during the formation of nuclei of future crystals, colloid formation was noted. After the specified synthesis time, the precipitate was filtered off and washed with hot hexane. Then it was dried in a desiccator to constant weight and identified by chemical and IR spectroscopic analysis. The IR spectrum of zinc sulfide is shown in Fig. 2. It corresponds to the data reported [42, 43]. According to the results of complexometric titration, the Zn content was (66.5 ± 0.4)% with its theoretical content in zinc sulfide being 67.1%. The sulfur content was determined by the gravimetric method [44]. It amounted to (31.4 ± 0.1)% with a theoretical sulfur content in zinc sulfide of 32.9%.

Synthesis of zinc sulfide doped with 0.050 at % of manganese ions (ZnS–Mn²⁺) was carried out using a similar method. Weighed amounts of zinc and manganese hexanoates were simultaneously placed into the reaction flask, and sulfur and dodecane were added. As the reaction progressed, a grayish-white precipitate

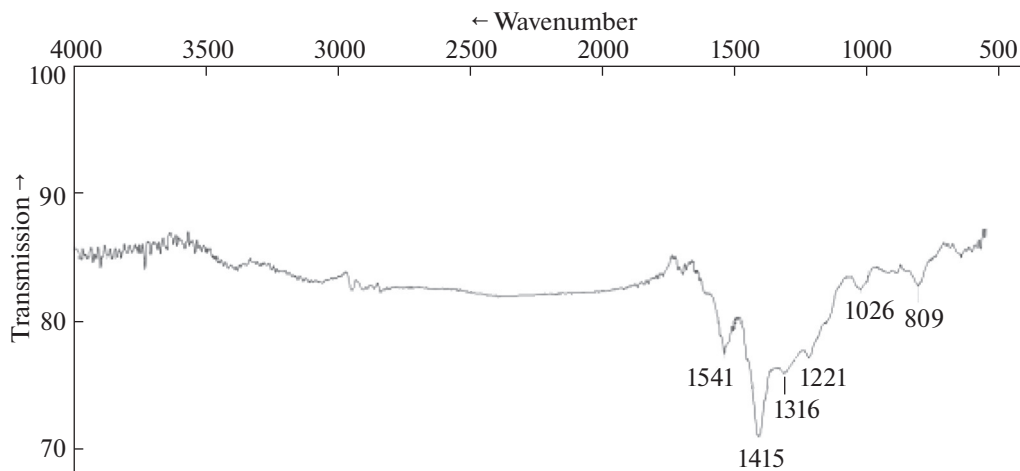


Fig. 2. IR spectrum of zinc sulfide (KBr tablet).

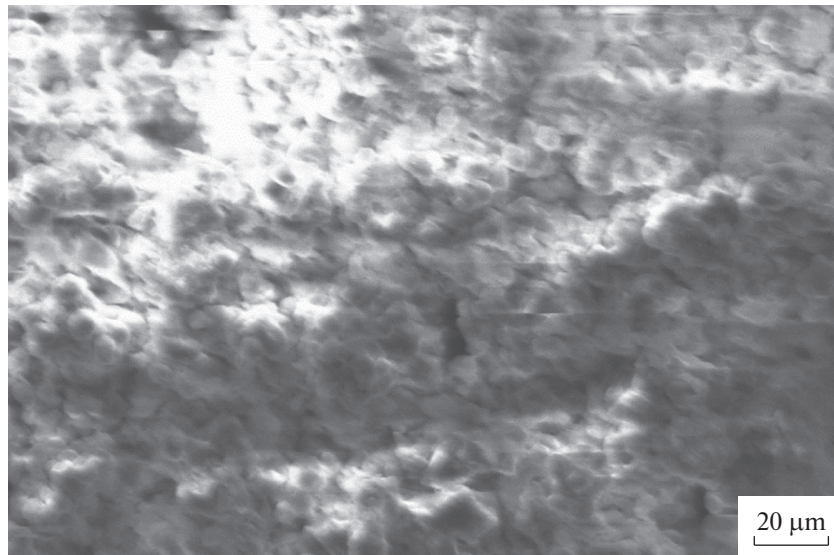


Fig. 3. Electronic photograph (SEM) of zinc sulfide powder.

was formed, which at the end of the synthesis was filtered off, washed with hot hexane, and dried in a desiccator to constant weight.

The microstructure of ZnS and ZnS–Mn was studied by electron microscopy on an EVO 50 scanning electron microscope (Carl Zeiss) with an Iridium Ultra probe microanalysis system (IXRF Systems). Images were obtained from the secondary electron detector (SE1) at an accelerating voltage of 10 or 20 kV. X-ray powder diffraction studies of product powders was carried out on an XRD-6000 diffractometer ($\text{Cu}K_{\alpha}$ radiation) using the PCPDFWIN databases and the POWDER CELL 2.4 full-profile analysis program. Diffuse reflectance, photoluminescence, and PL excitation spectra were recorded on a Shimadzu

RF-5301PC spectrofluorimeter according to the method reported [31].

RESULTS AND DISCUSSION

Electronic photographs of ZnS and ZnS–Mn powders are shown in Figs. 3, 4. Zinc sulfide powder consists of grains up to 8 μm in size of a distorted cubic shape with a fairly uniform size distribution (Fig. 3). A slight layer of structurally unformed compound is observed on the surface of the particles.

ZnS–Mn powder consists of globules that form round octahedral aggregates 10–100 μm in size; for example, see highlighted areas 1 and 2 (Fig. 4). The aggregates, in turn, are combined into larger elongated agglomerates; for example, see highlighted areas 2

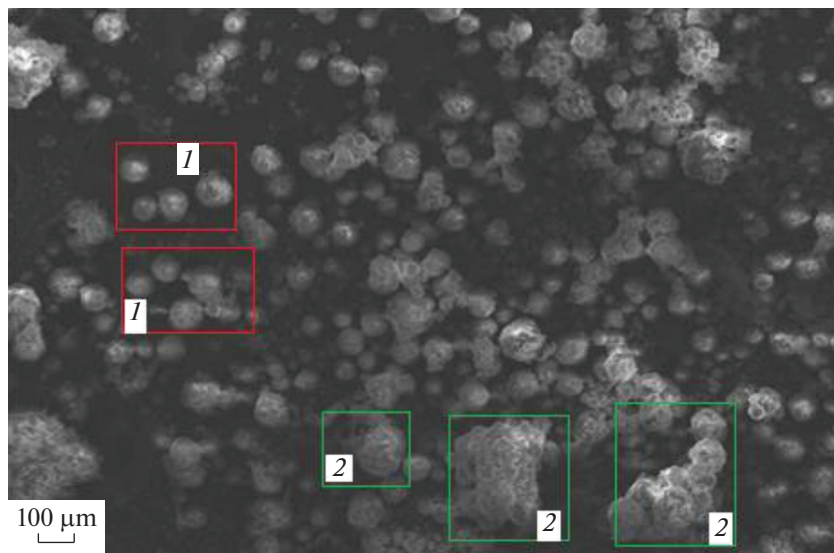


Fig. 4. Electronic photograph (SEM) of ZnS–Mn powder.

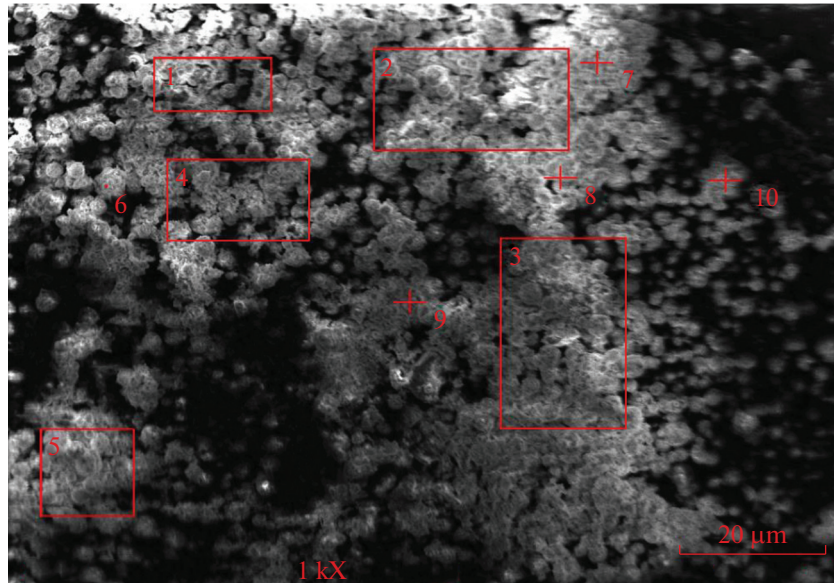


Fig. 5. Photograph indicating the locations of electron probe microanalysis of ZnS powder using unfocused (rectangles) and focused (crosses) X-ray radiation.

(Fig. 4). The surface of the globules, as in Fig. 3, is covered with a layer of slightly structured substance. The appearance of the particles (Figs. 3, 4) suggests the formation of polytypic crystals, including elements of cubic and hexagonal structural forms of zinc sulfide.

The results of electron probe microanalysis of ZnS and ZnS–Mn samples are shown in Figs. 5–8. The electronic photographs (Figs. 5, 7) highlight areas (rectangles) and points (crosses) of measurements, the size of which is $\sim 1 \mu\text{m}$. Typical energy dispersive spectra of ZnS and ZnS–Mn samples are shown in Figs. 6

and 8. The results of electron probe analysis confirm the elemental composition of the synthesis products, as well as their distribution on the surface of ZnS particles. The broadening of signals in the spectra may be associated with the structural heterogeneity of the substance, which, in turn, indirectly confirms the previously stated assumption about the polytype structure of the crystals being formed.

A detailed analysis of the process of formation of the ZnS structure is considered in review [8]. At the moment of particle nucleation and in particles whose size is a few nanometers, the possibility of the forma-

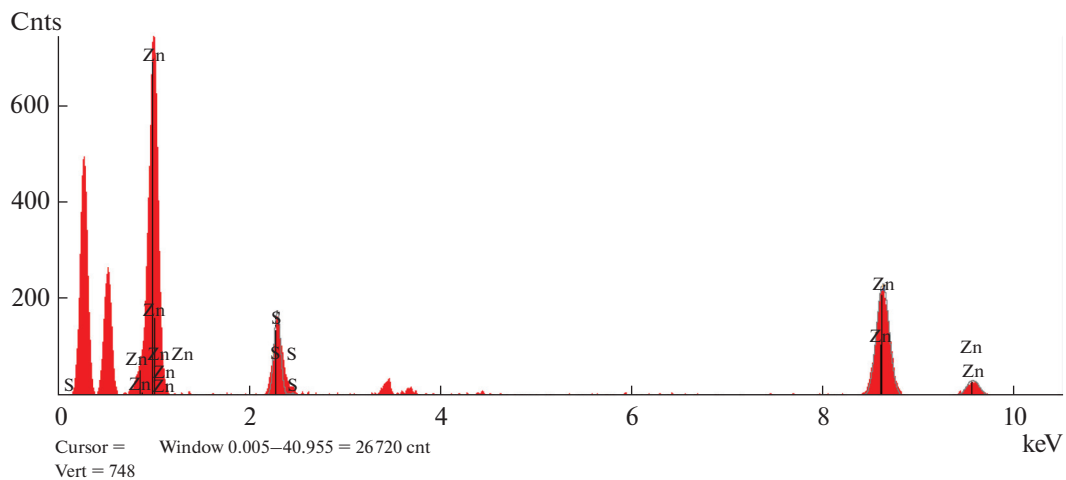


Fig. 6. Energy dispersive spectrum of the ZnS powder surface for recording region 1.

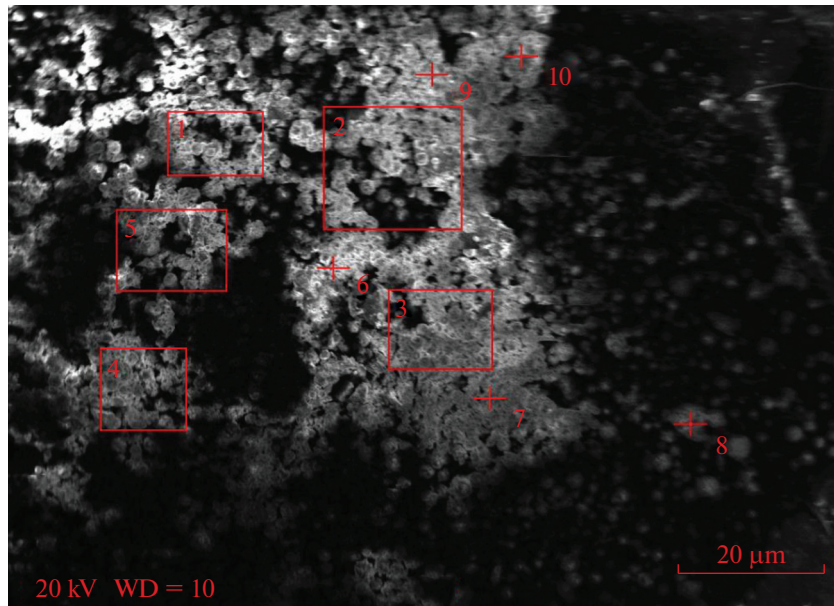


Fig. 7. Photograph indicating the locations of electron probe microanalysis of ZnS–Mn powder using unfocused (rectangles) and focused (crosses) X-ray radiation.

tion of a polytype layered structure of ZnS is noted [3, 6, 8, 45]. The authors [9] demonstrated the formation of ZnS films of cubic or hexagonal structure upon doping with various metals. It is noted that the type of structure formed depends on the type of doping cation [9]. For example, when doped with Cu^{2+} ions, crystals of doped ZnS of the cubic modification are formed; when doped with Fe^{2+} ions, crystals of the hexagonal modification are registered. The authors associate the formation of the structure with the concentration of the alloying component [9]. The synthesis from aqueous solutions and the results of studying cubic ZnS powders and ZnS/ Ag_2S heterostructures are given [46]. The

results of the synthesis and structural study of hexagonal ZnS films on carbon substrates are discussed [47].

The authors [45] synthesized ZnS powders by the microwave method in a water-ethanol medium when heated and studied the structure of the products depending on the synthesis temperature up to 150°C. According to the conclusions made based on a comparison of theoretical and experimental X-ray diffraction patterns, as well as spectroscopy results, hexagonal ZnS with space group $P63mc$ and particle size 2.6–3.7 nm was isolated [45]. At the same time, it is noted that it is difficult to identify products because of significant broadening, leading to overlapping reflections due to the small size of particles [45].

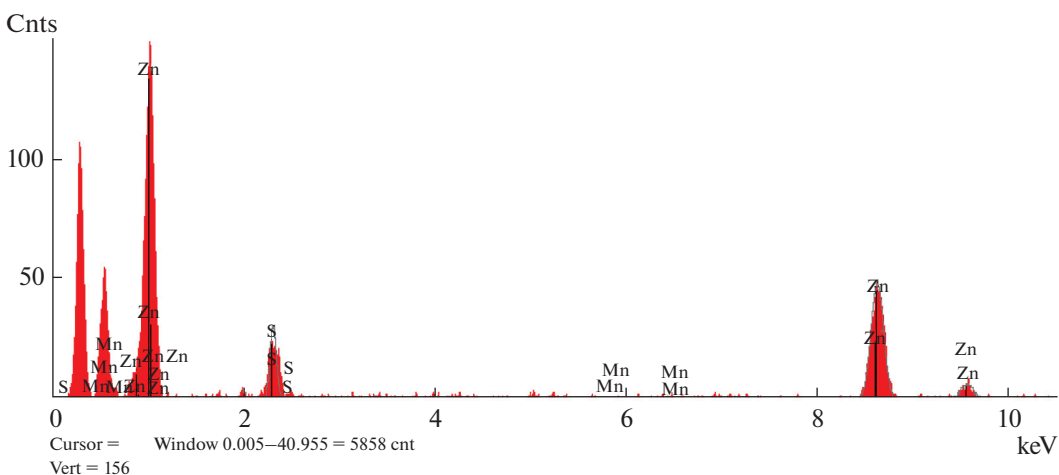


Fig. 8. Energy dispersive spectrum of the ZnS–Mn powder surface for recording region 1.

Experimental X-ray diffraction patterns of ZnS and ZnS–Mn powders synthesized in this work are shown in Figs. 9 and 10, respectively. Reflexes on radiographs are significantly broadened. The general appearance of the radiograph (Fig. 9) is close to the appearance of the radiographs reported [9, 45, 46]. Taking into account the data [9, 46, 47], it corresponds to a ZnS cubic structure with space group $F\bar{4}3m$. Calculation based on the formation of cubic ZnS gives a translational parameter value of 0.53814 nm. Its difference from the tabulated value of 0.54109 nm [46] resulted from the structure distortion. However, analysis of the X-ray diffraction pattern using the POWDER CELL 2.4 program, as performed [45], made it possible to identify in the product a ZnS phase of a hexagonal structure with a highly distorted lattice parameter $c = 3.1280$ nm being five times higher than the tabulated value of 0.6260 nm. The value of the parameter $a = 0.3803$ nm practically coincides with the table value equal to 0.3802 nm. The increase in the intensity of reflections in the region of 30° , 50° , and 60° is associated with the additive summation of intensities when overlapping bands of hexagonal and cubic crystals are superimposed. Against their background, the low-intensity band of hexagonal ZnS in the region of 52.5° (103) is practically invisible.

When comparing experimental results with data reported [9, 45–47], differences in synthesis conditions (dodecane, 216°C, 3.5 h) and in the state of the products (powders that have undergone the stage of colloid formation in an organic medium) were taken into account. In addition, the results of microscopy (the formation of particles on the surface of which a layer of weakly structured substance is observed (Figs. 3, 4)) and diffuse reflectance spectroscopy were taken into account. Based on this, it was concluded that crystals with a complex polytype structure are formed, united into agglomerates of size $<10 \mu\text{m}$ for ZnS and $<100 \mu\text{m}$ for ZnS–Mn.

This assumption is confirmed by the changes recorded in the X-ray powder diffraction pattern of ZnS–Mn (Fig. 10). After doping, a decrease in the band width is observed. This is probably due to better formation of the phases. According to microscopic analysis, the particle size in the ZnS–Mn system increases after agglomeration. In contrast to Fig. 9, the resolution of the multiplet in the region of 30° in the X-ray diffraction pattern of ZnS–Mn (Fig. 10) under the influence of manganese ions manifests itself to a greater extent, although it remains weakly expressed, differing from that presented in the X-ray diffraction patterns of doped ZnS films [9, 47]. This trend is also noted for high-angle reflections (Fig. 10). Full-profile X-ray powder diffraction pattern also shows the presence of a hexagonal ZnS phase. In addition, factors influencing the complication of bands in the X-ray diffraction pattern of ZnS–Mn (Fig. 10) may be the formation of local regions of manganese sulfide, leading to distortion of the crystal shape.

In the diffuse reflection spectrum of samples of ZnS and ZnS–Mn powders, an intense absorption band is observed at $\lambda < 250$ nm; the descending branch of this band extends to the region of 350 nm. The band at $\lambda < 250$ nm is associated with fundamental absorption of zinc sulfide. Absorption in the region > 280 nm corresponds to the formation of particles in the nanometer size range [1, 5, 21, 22, 31], which, apparently, form globules and agglomerates of various sizes observed in electronic photographs. The introduction of Mn²⁺ ions into zinc sulfide is manifested by an increase in the intensity of the band in the wavelength region > 300 nm. This circumstance is associated with an increase in the defectiveness of ZnS crystals when Mn²⁺ ions are present in their composition. The intrinsic absorption bands of Mn²⁺ ions do not appear in the spectrum due to their low concentration (0.050 at % Mn²⁺ ions) with low absorption coefficients corresponding to

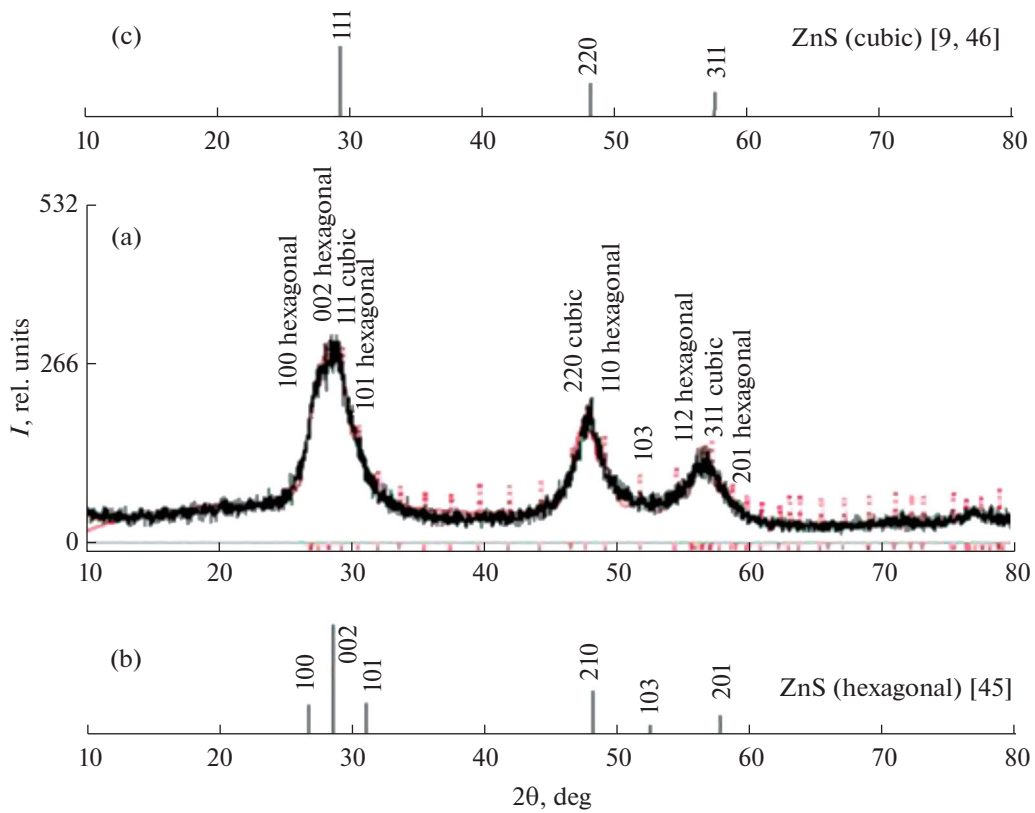


Fig. 9. Experimental X-ray powder diffraction pattern of ZnS powder: (a) assignment of reflections based on the presence of crystals of cubic and hexagonal structures; (b) assignment of reflections of hexagonal structure in accordance with study [45]; (c) assignment of reflections of cubic structure in accordance with works [9, 46].

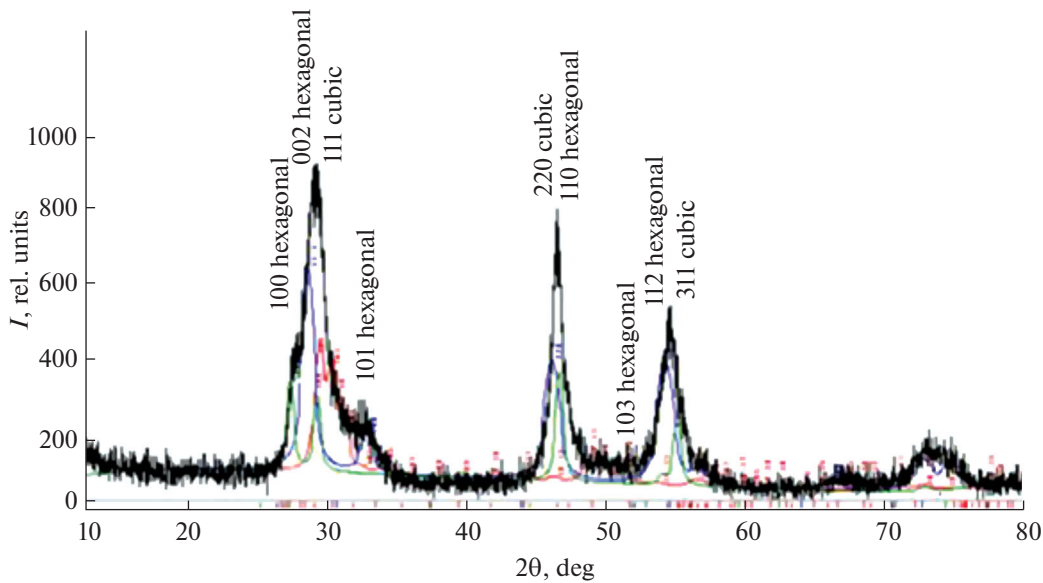


Fig. 10. X-ray powder diffraction pattern of ZnS–Mn powder.

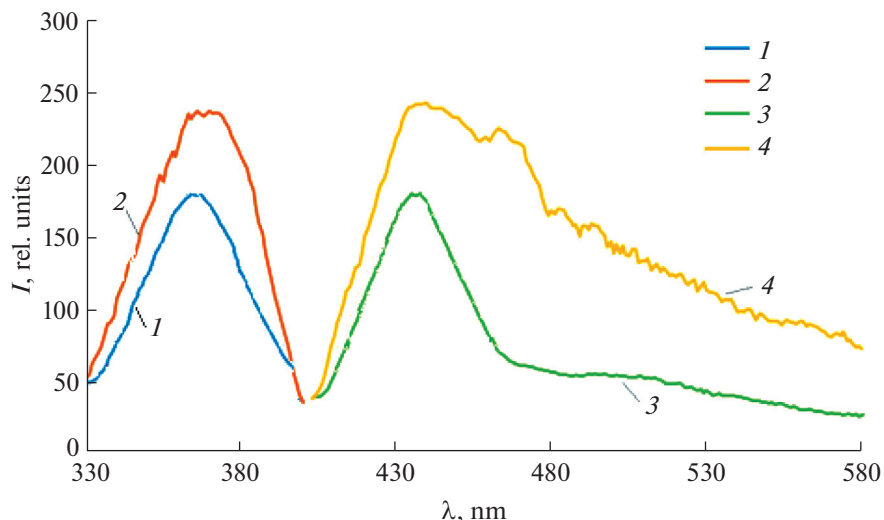


Fig. 11. Spectra of photoluminescence excitation (1, 2) and photoluminescence (3, 4) of ZnS samples ((1) for luminescence $\lambda_L = 450$ nm; (3) with excitation $\lambda_E = 360$ nm) and ZnS–Mn ((2) for luminescence $\lambda_L = 469$ nm; (4) with excitation $\lambda_E = 360$ nm).

Mn^{2+} ions. The results obtained are consistent with the data reported [31] for products of similar synthesis.

Photoluminescence of ZnS and ZnS–Mn powders was recorded upon photoexcitation by radiation corresponding to the absorption of primary particles in the nanoscale range of 360 nm (Fig. 11). Excitation spectra were recorded for 450 nm PL of ZnS powder and 469 nm PL of ZnS–Mn powder. In the second case, the bathochromic wavelength shift is associated with the course of the descending branch of the PL band under the influence of Mn^{2+} ions. Based on the position and type of band (Fig. 11, spectrum 3), the appearance of ZnS luminescence upon excitation by radiation with a wavelength of 360 nm can be explained by the occurrence of recombination processes at the levels of defects in semiconductor crystals [1, 19, 20, 26]. According to [14, 48], in the wavelength range 400–480 nm, the PL band is associated with singly negatively charged zinc vacancies (V'_{Zn}). Luminescence bands in the green region of the spectrum are associated with doubly charged zinc ion vacancies (V''_{Zn}) [1, 4] and sulfur vacancies (V_S) [14, 48, 49]. The band maximum (V_s) is assigned to a wavelength in the region of 520 nm [49]. In addition, at wavelengths >500 nm, bands associated with defects created by oxygen atoms are observed in the spectra. They quite easily occupy vacancies and replace atoms in the sites of the sulfur sublattice [50].

The region of excitation of ZnS luminescence corresponds to the transition of electrons from the valence band to the conduction band and to the levels of high-lying crystal defects. A significant inhomogeneous broadening of the bands in the luminescence and luminescence excitation spectra (Fig. 11, spectra 1 and 3) confirms the results presented above and the

corresponding conclusion about the inhomogeneity of the structure of the powder particles.

The PL band of ZnS–Mn powder is wider and more complex (Fig. 11, spectrum 4). Its descending branch is raised relative to the PL band of the ZnS powder (Fig. 11, spectrum 3). In the spectral region >450 nm, the influence of defect levels located low in the energy diagram of ZnS crystals, which are created by Mn^{2+} ions, is probably manifested. At long wavelengths, luminescence may appear, which is directly related to transitions between energy levels of manganese ions. The additivity of the intensities of the bands associated with these processes determines the course of the descending branch in the PL spectrum of the ZnS–Mn powder. The PL excitation band of ZnS–Mn powder (Fig. 11, spectrum 2) is bathochromically shifted relative to the PL excitation band of ZnS powder (Fig. 11, spectrum 1). This is due to the appearance of new defects and their corresponding energy levels on the zinc sulfide diagram.

CONCLUSIONS

In this work, zinc sulfide powder doped with Mn^{2+} ions was synthesized using the method of emerging reagents in a homogeneous dodecane medium. The elemental composition, structure, and morphology of the powder were studied by electron microscopy using microprobe analysis, X-ray powder diffraction, and chemical analysis. The appearance of the diffuse reflection, PL excitation, and photoluminescence spectra of samples of ZnS and ZnS–Mn powders confirms the conclusion about the multilevel polytype structure of the substance and allows us to make assumptions about the reasons for the occurrence of PL of the samples.

ACKNOWLEDGMENTS

The authors thank the staff of the Interregional Center for Collective Use of the Tomsk State University for recording the X-ray spectra and ZAO “SuperOx” (Moscow, Russia) for conducting electron microscopic studies of the synthesized samples.

FUNDING

This work was supported by ongoing institutional funding. No additional grants to carry out or direct this particular research were obtained.

CONFLICT OF INTEREST

The authors declare that they have no conflicts of interest.

REFERENCES

1. R. F. Khairutdinov, Russ. Chem. Rev. **67**, 109 (1998).
2. N. M. Sergeeva, S. P. Bogdanov, and Sh. O. Omarov, Izv. SPbGTI (TU) **46**, 56 (2018).
3. A. A. Rempel, Russ. Chem. Rev. **76**, 435 (2007). <https://doi.org/10.1070/RC2007v07n05ABEH003674>
4. W. Lu, X. Guo, Y. Luo, et al., Chem. Eng. J. **355**, 208 (2019). <https://doi.org/10.1016/j.cej.2018.08.132>
5. E. Ramya, M. V. Rao, and D. N. Rao, Physica E **107**, 24 (2019). <https://doi.org/10.1016/j.physe.2018.11.010>
6. S. I. Sadovnikov, A. V. Ishchenko, and I. A. Weinstein, Russ. J. Inorg. Chem. **65**, 1312 (2020). <https://doi.org/10.1134/S0036023620090144>
7. S. Kumar, R. Bhushan, S. R. Kumar, and S. Rajpal, Chalcogen. Lett. **19**, 1 (2022). <https://doi.org/10.15251/CL.2022.191.1>
8. S. I. Sadovnikov, Russ. Chem. Rev. **88**, 571 (2019). <https://doi.org/10.1070/RCR4867?locatt=label:RUSSIAN>
9. M. A. Shakil, S. Das, M. A. Rahman, et al., Mater. Sci. Appl. **9**, 751 (2018). <http://www.scirp.org/journal/msa>.
10. T. Hurma, J. Mol. Struct. **1161**, 279 (2018). <https://doi.org/10.1016/j.molstruc.2018.02.070>
11. L. N. Maskaeva, A. D. Kutyavina, V. F. Markov, et al., Russ. J. Gen. Chem. **88**, 295 (2018). <https://doi.org/10.1134/S1070363218020172>
12. A. D. Selyanina, L. N. Maskaeva, V. I. Voronin, et al., Russ. J. Inorg. Chem. **68**, 26 (2023).
13. L. N. Maskaeva, V. F. Markov, V. I. Voronin, et al., Inorg. Mater. **59**, 419 (2023). <https://doi.org/10.31857/S0002337X23040061>
14. O. N. Kazankin, L. Ya. Markovskii, I. A. Mironov, et al., *Inorganic Phosphors* (Khimiya, Leningrad, 1975) [in Russian].
15. R. N. Bhargava, D. Gallagher, X. Hong, and A. Nurmiikko, Phys. Rev. Lett. **72**, 416 (1994).
16. V. G. Korsakov, M. M. Sychev, ad V. V. Bakhmet'ev, Kondens. Sredy Mezhpaz. Gran. **14**, 41 (2012).
17. K. A. Ogurtsov, M. M. Sychov, V. V. Bakhmetyev, et al., Inorg. Mater. **52**, 1115 (2016). <https://doi.org/10.1134/S0020168516110121>
18. A. A. Othman, M. A. Osman, M. A. Ali, et al., J. Mater. Sci.—Mater. Electron. **31**, 1752 (2020). <https://doi.org/10.1007/s10854-019-02693-z>
19. T. V. Vineeshkumar, D. Rithesh Raj, S. Prasanth, et al., Opt. Mater. **37**, 439 (2014). <https://doi.org/10.1016/j.optmat.2014.06.037>
20. J. K. Saluja, Y. Parganiha, N. Tiwari, et al., Optik, **127**, 7958 (2016). <https://doi.org/10.1016/j.ijleo.2016.05.011>
21. Y. G. Galyametdinov, D. O. Sagdeev, V. K. Voronkova, et al., Rus. Chem. Bull. **67**, 172 (2018). <https://doi.org/10.1007/s11172-018-2055-1>
22. D. O. Sagdeev, *Extended Abstract of Cand. Sci. (Chem.) Dissertation*, Kazan, 2019.
23. N. H. Patel, M. P. Deshpande, S. H. Chaki, and H. R. Keharia, J. Mater. Sci.—Mater. Electron. **28**, 10866 (2017).
24. M. F. Bulanuy, A. V. Kovalenko, B. A. Polezaev, and T. A. Prokof'yev, Semiconductors **43**, 16 (2009). <https://doi.org/10.1134/S1063782609060050>
25. B. N. Litvin and V. I. Popolitov, *Hydrothermal Synthesis of Inorganic Compounds* (Nauka, Moscow, 1984) [in Russian].
26. D. Denzler, M. Olszewski, and K. Sattler, J. Appl. Phys. **84**, 2841 (1998).
27. P. Kunstman, J. Coulon, O. Kolmykov, et al., J. Luminesc. **194**, 760 (2018). <https://doi.org/10.1016/j.jlumin.2017.09.047>
28. A. A. Zarubanov and K. S. Zhuravlev, Semiconductors **49**, 380 (2015). <https://doi.org/10.1134/S1063782615030252>
29. V. P. Smagin, D. A. Davydov, N. M. Unzhakova, and A. A. Biryukov, Russ. J. Inorg. Chem. **60**, 1588 (2015). <https://doi.org/10.1134/S0036023615120244>
30. A. A. Isaeva and V. P. Smagin, Russ. J. Inorg. Chem. **64**, 1199 (2019). <https://doi.org/10.1134/S0036023619100061>
31. L. V. Zatonskaya, V. P. Smagin, E. P. Harnutova, and E. V. Ignatov, Semiconductors **56**, 411 (2022). <https://journals.ioffe.ru/articles/viewPDF/5354>.
32. E. I. Perov and E. P. Irkhina, Inorg. Mater. **33**, 657 (1997).
33. E. I. Perov, E. P. Irkhina, E. G. Il'ina, et al., Patent RF 2112743.
34. E. P. Irkhina, *Extended Abstract of Cand. Sci. (Chem.) Dissertation*, Barnaul, 2000.
35. N. V. Moshchenskaya, I. V. Deryabina, and E. I. Perov, Izv. AltGU **3**, 19 (2000).
36. E. P. Kharnutova and E. I. Perov, Izv. AltGU **3-2**, 186 (2010).

37. E. G. Il'ina, V. P. Smagin, L. V. Zatonskaya, and E. P. Kharnutova, Polzun. Vest. **2**, 107 (2020).
<https://doi.org/10.25712/ASTU.2072-8921.2020.02.020>
38. E. G. Il'ina, N. A. Santalova, and K. M. Dunaeva, Zh. Neorg. Khim. **36**, 1297 (1991).
39. A. J. Gordon and R. A. Ford, *The Chemist's Companion: A Handbook of Practical Data, Techniques, and References* (John Wiley and Sons, Inc., New York, 1973).
40. V. P. Zhivopistsev and E. A. Selezneva, *Analytical Chemistry of Zinc* (Nauka, Moscow, 1975) [in Russian].
41. K. A. Lavrukhina and L. V. Yukina, *Analytical Chemistry of Manganese* (Nauka, Moscow, 1974) [in Russian].
42. A. M. Kharkov, M. N. Sitnikov, O. B. Begisheva, et al., IOP Conf. Ser.: Mater. Sci. Eng. 1118 (2021).
43. E. V. Karaksina, *Extended Abstract of Doctoral Sci. (Chem.) Dissertation*, Nizhny Novgorod, 2004.
44. V. I. Fadeeva, G. N. Shekhtovtsova, V. I. Ivanov, et al., *Fundamentals of Analytical Chemistry* (Vysshaya Shkola, Moscow, 2001) [in Russian].
45. A. N. Kravtsova, A. P. Budnik, A. A. Tsaturyan, et al., J. Struct. Chem. **58**, 1397 (2017).
46. S. I. Sadovnikov and I. D. Popov, Phys. Solid State **62**, 2004 (2020).
47. W.-H. Liao, Q.-Q. Hu, M. Cheng, et al., RSC Adv. **11**, 33344 (2021).
<https://doi.org/10.1039/d1ra06427d>
48. T. A. Kuchakova, G. V. Vesna, and V. A. Makara, Semiconductors **38**, 1275 (2004).
<https://doi.org/10.1134/1.1823058>
49. Yu. Yu. Bacherikov, I. P. Vorona, and S. V. Optasyuk, Semiconductors **38**, 987 (2004).
<https://doi.org/10.1134/1.1797471>
50. N. K. Morozova, I. A. Karetnikov, D. A. Mideros, et al., Semiconductors **40**, 1155 (2006).
<https://doi.org/10.1134/S106378260610006X>

Translated by V. Avdeeva

Publisher's Note. Pleiades Publishing remains neutral with regard to jurisdictional claims in published maps and institutional affiliations.